EARTH SURFACE PROCESSES AND LANDFORMS
Earth Surf. Process. Landforms **43**, 172–186 (2018)
Copyright © 2017 John Wiley & Sons, Ltd.
Published online 14 July 2017 in Wiley Online Library
(wileyonlinelibrary.com) DOI: 10.1002/esp.4166

Topographic forcing of tidal sandbar patterns for irregular estuary planforms

J. R. F. W. Leuven,* T. de Haas, L. Braat and M. G. Kleinhans
Faculty of Geosciences, Utrecht University, Utrecht, The Netherlands

Received 17 October 2016; Revised 17 April 2017; Accepted 19 April 2017

*Correspondence to: J. R. F. W. Leuven, Faculty of Geosciences, Utrecht University, Utrecht, The Netherlands. E-mail: j.r.f.w.leuven@uu.nl
This is an open access article under the terms of the Creative Commons Attribution License, which permits use, distribution and reproduction in any medium, provided the original work is properly cited.

ESPL
Earth Surface Processes and Landforms

ABSTRACT: Estuaries typically show converging planforms from the sea into the land. Nevertheless, their planform is rarely perfectly exponential and often shows curvature and the presence of embayments. Here we test the degree to which the shapes and dimensions of tidal sandbars depend on estuary planform. We assembled a dataset with 35 estuary planforms and properties of 190 tidal bars to induce broad-brush but significant empirical relations between channel planform, hydraulic geometry and bar pattern, and tested a linear stability theory for bar pattern. We found that the location where bars form is largely controlled by the excess width of a channel, which is calculated as the observed channel width minus the width of an ideal exponentially widening estuary. In general, the summed width of bars approximates the excess width as measured in the along-channel variation of three estuaries for which bathymetry was available as well as for the local measurements in the 35 investigated estuaries. Bar dimensions can be predicted by either the channel width or the tidal prism, because channel width also strongly depends on local tidal prism. Also braiding index was predicted within a factor of 2 from excess width divided by the predicted bar width. Our results imply that estuary planform shape, including mudflats and saltmarsh as well as bar pattern, depend on inherited Holocene topography and lithology and that eventually convergent channels will form if sufficient sediment is available. Copyright © 2017 John Wiley & Sons, Ltd.

KEYWORDS: estuary; tidal bars; bar pattern; braiding index; convergence; hydraulic geometry

Introduction

Estuaries are converging bodies of water that have inflow of river water at the landward boundary and an open connection to the sea. In ideal estuaries, the tidal range, average depth and current velocity amplitude are uniform in the along-channel direction, whereas the channel width exponentially converges in the landward direction (Pillsbury, 1956; Langbein, 1963; Savenije, 2015). Ideal estuary behaviour has been argued to arise when an estuary has adapted its shape to the boundary conditions by sedimentation and erosion (Townend, 2012, Savenije, 2015). However, this requires that (i) the estuary has adapted to Holocene sea-level rise, (ii) sufficient sediment and time were available for the adaptation and (iii) the antecedent topography could adapt, which excludes substrates that are erosion resistant. Therefore, estuaries in nature are expected to exhibit varying degrees of adaptation towards ideal estuaries, where embayments are partially filled with sandbars, mudflats and saltmarshes, and where the overall planform is partly determined by antecedent geology (Townend, 2012) (Figure 1).

The planform of estuaries typically converges from the seaward side to the landward side. Within this planform, the dimensions of tidal bars and the number of parallel channels gradually vary, often decreasing in the landward direction. However, due to sea-level rise, sediment supply and time for adaptation, the estuary shape deviates from an ideal shape. This has major implications for tidal wave propagation and sediment transport, because it alters the hydrodynamics and net sediment transport over time (Friedrichs and Aubrey, 1994; van den Berg *et al.* 1996; Lanzoni and Seminara, 1998; Savenije, 2006) and in addition it influences the bar patterns. For example, the mouth of an estuary may be confined by a sand spit, followed by a long and wide compound bar at the landward side (Figure 1a, b). At locations where the estuary is wide, bar dimensions and braiding index generally increase. At the landward end, the number of channels generally reduces towards a single threaded river (Figure 1).

Here we focus on funnel shaped non-ideal alluvial estuaries with dynamic patterns of channels and sandbars, often flanked by tidal mudflats and saltmarshes. We investigate the effects of natural deviations from the ideal estuary shape, such as embayments, on the bar pattern. Furthermore, we analyse how channel planform of non-ideal estuaries topographically forces patterns of tidal bars. It was previously found that tidal bar dimensions depend mostly on the channel width, measured as the width between the vegetated marshes or banks including the sandbars (Leuven *et al.*, 2016). In addition, the location of bars in the similar environment of rivers can be forced by embayments, bends and other planimetric non-uniformities (Tubino *et al.*, 1999; Seminara, 2010; Schuurman *et al.*, 2013). At locations along an estuary or river where the width of the cross-section increases, the stream

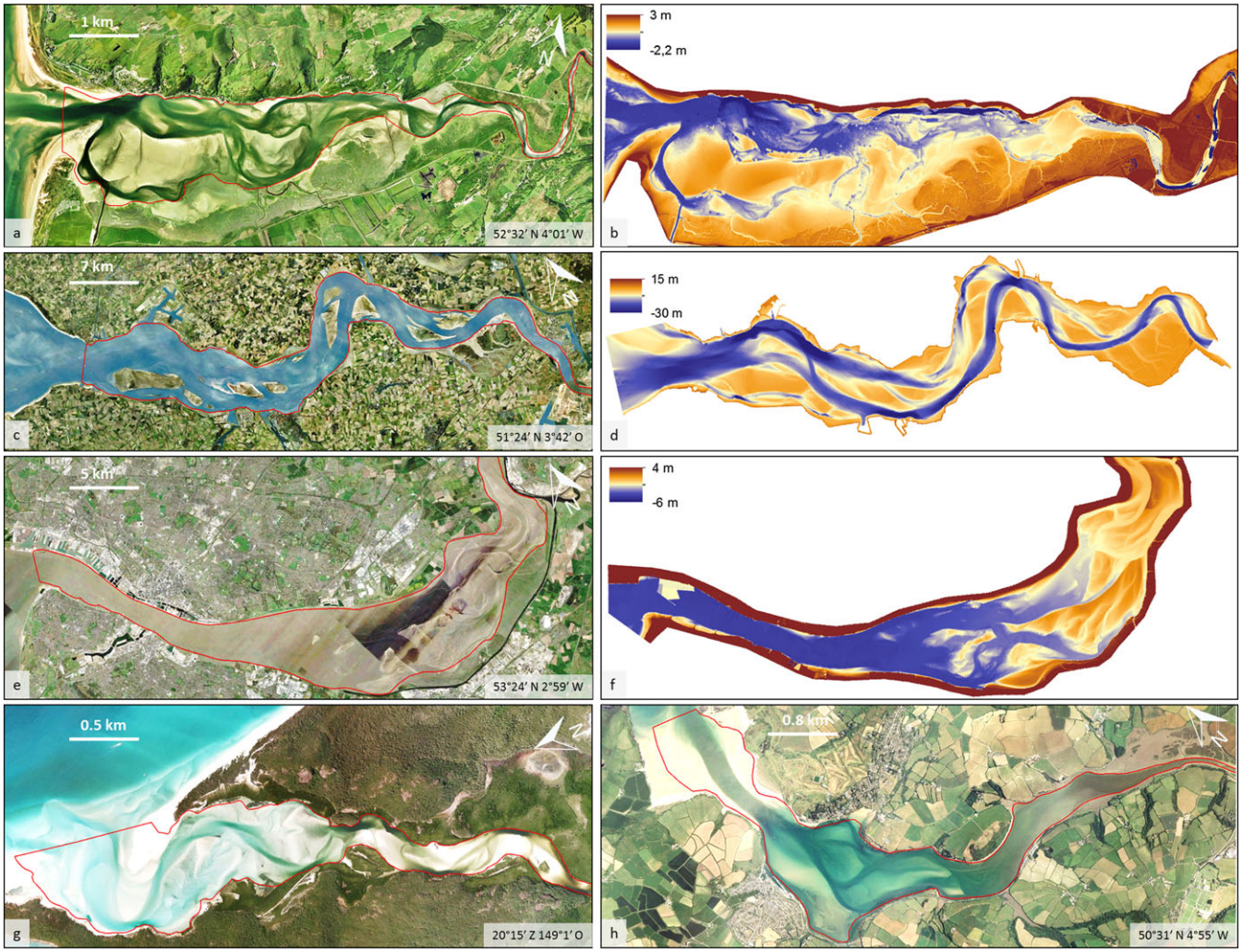

Figure 1. Aerial photographs of estuaries and available bathymetries. (a, b) Dovey estuary (UK); (c, d) Western Scheldt (NL); (e, f) Mersey estuary (UK); (g) Whitehaven beach (Australia); (h) Camel estuary (UK). Red lines represent digitized channel planforms. Images: Google Earth, accessed January–September 2016. [Colour figure can be viewed at wileyonlinelibrary.com]

velocity generally decreases and hence the shear stress, which favours sediment deposition. These observations and theory suggest that sandbar patterns in estuaries partly depend on the present planform shape of the estuary.

For bar pattern in rivers, bars are either classified as free or as forced. While forced bars are forced to their location by the planform shape of the channel, free bars can migrate freely and occur in straight or weakly curved channels (Tubino *et al.*, 1999; Seminara, 2010; Schuurman *et al.*, 2013). It was found that the topographic forcing of bars occurs on (i) the scale of individual bars, due to meander bends and embayments, which fix the bars at their location (Struiksma *et al.*, 1985; Repetto and Tubino, 2001; Wu *et al.*, 2011) and (ii) the reach scale, an order of magnitude larger than individual bars, due to variations in channel width and discharge (Tubino *et al.*, 2011; Seminara, 2010; Kleinhans and van den Berg, 2011; Schuurman *et al.*, 2013). For rivers, the latter scale sets independent variables that determine bar pattern. In addition, the channel width may be non-uniform in space, causing local flow expansion or convergence to force the formation of bars. Since estuaries generally have converging channels, we define the non-uniformity of estuary channel width here as the deviation from an ideal exponential profile. Nevertheless, it is unknown whether the forcing mechanisms for rivers extend to estuaries. Therefore, we record and analyse forced bars in non-ideal alluvial estuaries in this study, to determine how non-uniformity affects the location, shape and dimensions of tidal bars.

Our work partly builds on previous research that mainly focused on the dimensions and shapes of individual tidal bars and how they compare to theoretical predictions (Leuven *et al.*, 2016). We found that tidal bar dimensions increase with estuary dimensions, in particular with estuary channel width (e.g. bar length $\propto$ channel width$^{0.87}$). This result contradicts classical tidal bar theory, which predicts that tidal current velocity – or tidal excursion length – determines bar length (Seminara and Tubino, 2001; Schramkowski *et al.*, 2002). The research of Leuven *et al.* (2016) forms a starting point to study the along-channel variation in bar pattern, for which predictive relations are still lacking. To obtain a prediction of the bar pattern on the estuary scale, it is required to predict the along-channel variation in the braiding index and the location where bars form. Obtaining these relations will thus be the main focus of this paper. If relations for individual bar dimensions are required, we rely on the data and relations presented in Leuven *et al.* (2016).

While Leuven *et al.* (2016) showed that theory mispredicts the dimensions of individual bars, it still is the only method to obtain a first idea of the along-channel variation in bar pattern in estuaries up to the present day. Figure 2 shows a prediction of the along-channel summed width of bars and braiding index (BI) for the Western Scheldt (NL) according to theories

Copyright © 2017 John Wiley & Sons, Ltd.

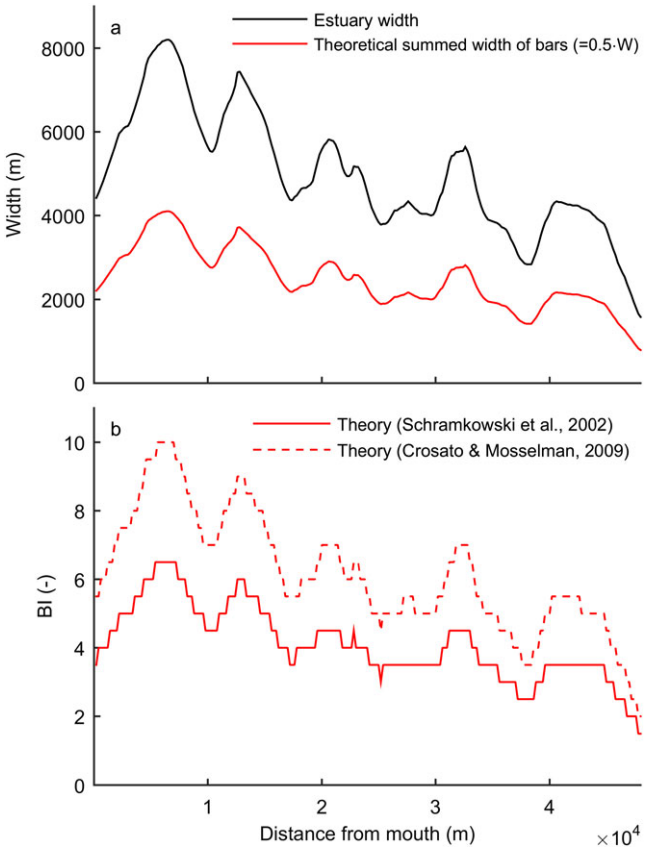

Figure 2. Theoretical prediction of summed width of bars (a) and braiding index (b) from channel width, in this case of the Western Scheldt, by the linear stability theories of Schramkowski *et al.* (2002) and Crosato and Mosselman (2009), following the approach in Leuven *et al.* (2016). [Colour figure can be viewed at wileyonlinelibrary.com]

of Schramkowski *et al.* (2002) and Crosato and Mosselman (2009). Since theoretical approaches describe tidal bars as wave forms, they predict the summed width of all individual bars to be approximately equal to half the channel width by definition (Figure 2), which probably overestimates the formation of bars at points where the estuary is confined by bedrock geology or human influence. While the theoretical predictions form a starting point for this study, our aim is to improve the predictions using an empirical method. The previous empirical study (Leuven *et al.*, 2016) and forcing mechanisms for rivers (Tubino *et al.*, 1999; Seminara, 2010; Kleinhans and van den Berg, 2011; Schuurman *et al.*, 2013) imply that to understand the along-channel variation in bar pattern for estuaries it is necessary to take their converging planform and local variations in width and discharge into account.

The relation between bar dimensions and channel geometry raises the question of what the local geometry of an estuary determines. Hydraulic geometry describes relations between discharge, channel width, depth and flow velocity. Previously, relations were derived for specific tidal systems (Sassi *et al.*, 2012; Gisen and Savenije, 2015; Lanzoni and D'Alpaos, 2015) and as a function of independent, external boundary conditions, in particular river discharge, tidal amplitude and estuary mouth dimensions (Davies and Woodroffe, 2010; Townend, 2012). For rivers, it was shown that channel forming or bankfull discharge is an appropriate indicator to predict channel width (Lacey, 1930; Leopold and Maddock, 1953; Hey and Thorne, 1986; Savenije, 2003; Kleinhans and van den Berg, 2011). In estuaries, discharge varies significantly over a tidal cycle. Therefore, we expect that the channel-forming discharge for estuaries may be approximated by the average volume of water flowing through a cross-section over half a tidal period. This was demonstrated to be a good predictor for hydraulic geometry in multiple tidal systems (e.g. O'Brien, 1969; Eysink, 1990; Friedrichs, 1995; Lanzoni and D'Alpaos, 2015) and it may therefore also serve as a predictor for bar patterns.

Our aim is to assess the degree to which bar patterns depend on the irregularities in the planform width of estuaries as far as this deviates from the ideal, exponentially converging, shape. We test the hypothesis that the topography, in particular channel width, forces the bar pattern and that local tidal prism predicts the hydraulic geometry of estuaries. Therefore, we assembled a dataset with the planform of 35 estuaries, analysed the effect of planform on bar pattern and compared it with the results from theoretical predictions.

The paper is organized as follows. First, the methodology is given for collecting bar pattern and estuary planform data. Second, we describe empirical relations between tidal bar properties and planform shape of estuaries. Then, the empirical results are compared with theoretical predictions. The applicability of the results is discussed for cases where little data is available, such as the reconstruction of bar patterns in former Holocene estuaries.

Methods

This study partly builds on the previously collected dataset of Leuven *et al.* (2016), which was focused on the dimensions and shapes of individual bars only. We first summarize this dataset with its underlying assumptions and uncertainties, as far as relevant for this study. Thereafter, it is described how this dataset was extended to enable a study of the bar pattern on the estuary scale. To do so, measurements of the summed width of bars were made and channel planforms were collected. Finally, we describe the methodology for data processing and definitions used in the results.

Available dataset

Leuven *et al.* (2016) assembled a dataset with local measurements of individual tidal bars and collected detailed bathymetries for three estuaries: the Western Scheldt (NL), Dovey (UK) and Mersey (UK) (Figure 1b, d, f). Data for the Western Scheldt was obtained from Rijkswaterstaat, for the Dovey estuary from Aberystwyth University (Wales) and for the Mersey from the UK government. In addition, geomorphological maps were available for the Western Scheldt with ecotopes, obtained from Rijkswaterstaat (NL) (Figure 3c). Most of the estuaries for which bar dimensions were measured are located in the USA and Western Europe.

The dataset contains the dimensions (length, width and height) of 190 tidal bars in 45 funnel-shaped alluvial estuaries and included data on estuarine properties (Figure 4). Based on their shape, the bars were classified into four classes: sidebars, linear bars, u-shaped bars and compound bars (Figure 4). Analyses of the dataset showed that compound bars and u-shaped bars can be seen as simple linear bars partly cut by barb channels, where a barb channel is defined as a one-ended channel that partly cross-cuts the bar and becomes shallower in the direction of flow (Dalrymple and Choi, 2007; Leuven *et al.*, 2016). Therefore, we previously introduced two measures of bar width: the maximum bar width and the partitioned bar width. The maximum bar width was recorded at the local maximum of individual bars (Figure 4). The partitioned bar width was calculated as the maximum bar width divided

Copyright © 2017 John Wiley & Sons, Ltd.

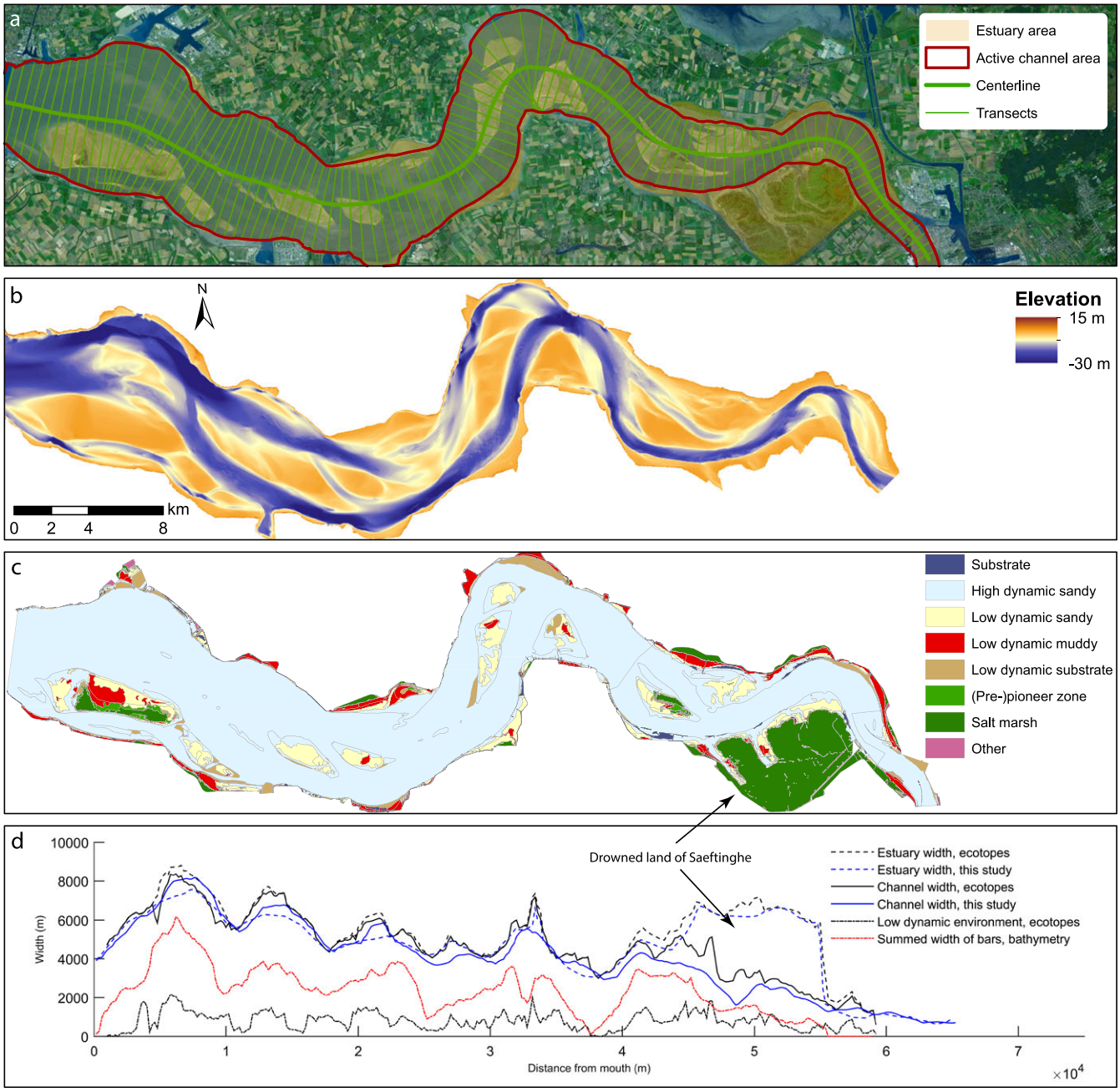

Figure 3. Illustration of the methodology to collect channel and estuary planform and channel width along the Western Scheldt. Given the focus on bars, the mudflats and saltmarshes are excluded from the channel planform width. (a) Aerial photograph with the definitions used in this study: estuary area, active channel area, centreline of active channel area and transects. Bing Maps, accessed September 2016. (b) Bathymetry and (c) ecotope map of the Western Scheldt (2012), obtained from Rijkswaterstaat. (d) Estuary width, channel width, bar width and low dynamic environments as derived from the polygons drawn on the aerial photograph, the bathymetry and ecotope map. [Colour figure can be viewed at wileyonlinelibrary.com]

by the number of barb channels (Figure 4). In the present study, we add the measure of the summed width of bars to these definitions. The summed width of bars is defined as the sum of all bar widths in one cross-section (see Figure 4 for an example).

In the dataset, estimations were made for the local channel depth at the tidal bar locations. To do so, a linear depth profile was assumed between the mouth of the estuary and upstream river depth. To validate this, the measurements of the average channel depth excluding bars were compared with the assumption of a linear increasing bed profile for the three cases for which bathymetry was available (the Dovey, Mersey and Western Scheldt estuary). It was found that the predictions with this assumption are within 10% of the measured value. The Western Scheldt formed an exception, because its channels are dredged. The cross-sectional channel area at the bar locations was estimated in this study. To do so, the estimated average channel depth excluding bars from Leuven *et al.* (2016) was multiplied by the channel width excluding bars. The error of maximum 10% in the prediction of channel depth is linearly propagated in our estimations of cross-sectional area.

As the dataset was collected from aerial photographs, the precise water level with respect to mean sea level was unknown for the moment the aerial photograph was taken. Since the water level influences the apparent bar shape observed from aerial photographs, Leuven *et al.* (2016) analysed the likely measurement error that arises from the unknown flow stage. It was found that bar length and width measured at mean sea level and low water level are at most a factor of 2 larger or smaller than when measured at the

Copyright © 2017 John Wiley & Sons, Ltd.

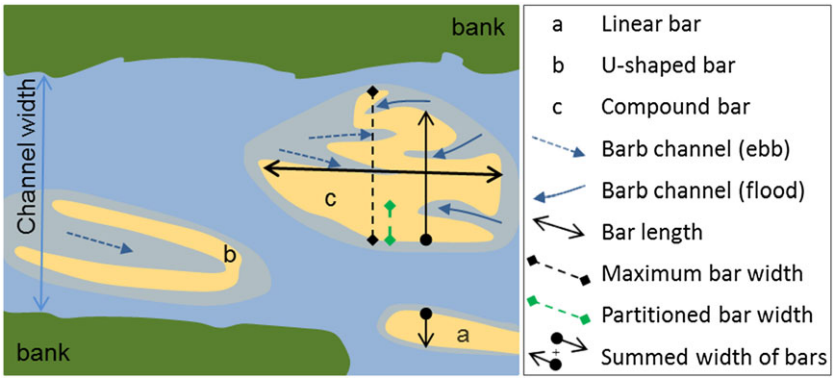

Figure 4. Schematic of a linear bar, u-shaped bar and compound bar with the corresponding measurements of channel width, bar length, maximum bar width, partitioned bar width and summed width of bars. Barb channels are channels that become shallower in the direction of flow and taper out onto the bar regardless of water level, while flow during high water diverges out of the barb channel. The summed width of bars is the sum of all bar widths in one cross-section. [Colour figure can be viewed at wileyonlinelibrary.com]

exact intermediate water level, which is smaller than the scatter within the full dataset for which the trends that were found span multiple orders of magnitude.

Planform classification and data collection

For 35 of the 45 estuaries in the dataset of Leuven *et al.* (2016), a polygon of the outline of the estuary planform was recorded (supplementary Table B.1), which covered 170 of the 190 bars in the original dataset. At these 170 locations the summed width of bars was measured from aerial photography. Due to a lack of bathymetries for estuaries, channel planform was visually recorded using Google Earth, based on the morphology visible on aerial photography. This approach is similar to the classification of ecotopes on the geomorphological map of the Western Scheldt (de Jong, 1999; Bouma *et al.*, 2005). Nevertheless, it excludes any *in situ* measurements such as salinity and mud content and therefore relies more on visual observations.

Ideally, the polygons would extent up to the tidal limit. However, it is impossible to derive the tidal limit from an aerial photograph, and detailed depth profiles to estimate this are lacking. Therefore, the polygons were digitized over the extent for which mutually evasive ebb and flood tidal channels were present and we included the first single-thread meander. Below, we assess how this influences our approximation of the tidal prism. For each estuary, two types of planform polygons were recorded: the active channel polygon and the estuary polygon (Figure 3a).

Active channel area refers to the area with a dynamic pattern of channels and sandbars, and is approximately the area that is submerged at mean sea level. This means that we here exclude the mudflats and saltmarshes from the active bar pattern. The active channel planform covers the part of the estuary in which large (>100s of metres) dynamic channels and bars that lack mud and vegetation are present (Figure 3a). In this area, the orientation of channels and bars is parallel to the centreline. The channel orientation, together with the dimensions of the channel, indicates that substantial sediment transport occurs in the along-channel direction. The presence of bedforms and barb channels and the absence of vegetation was used as an indicator of the active channel area, where sediment is regularly transported and vegetation cannot sustain.

Estuary area refers to the area that is approximately submerged during mean sping tide. The estuary area covers the active channel area plus the vegetated marshes, flats and former abandoned estuarine areas. These areas were classified based on the presence of dense vegetation or a muddy layer of surface sediment that is darker than the sediment on the tidal bars. In addition, these areas were often dissected by small (<100s of metres) channels perpendicular to the centreline. The presence of vegetation or pioneering vegetation indicates that the tidal flats are only submerged and active during the highest water levels. The spatial transitions from pioneering vegetation to forest, bedrock geology or human-dominated landscape were used as the maximum extent for the estuary area.

The summed width of bars was measured on the same aerial photograph as for which the polygons were digitized. For some cases these differ from the date of the aerial photographs used in Leuven *et al.* (2016) (Table C.3, supporting information). These measurements were added to the dataset of Leuven *et al.* (2016).

The supplementary material, provided online as supporting information, contains the active channel area polygons (Table D.4) and a list of estuaries used in this study (supplementary Table B.1), including measurements of the approximate surface areas of the estuary area. Because the active channel planform may change over time, the date of the aerial photograph is given for the recorded planforms (supplementary Table B.1). To optimize classification and recording, photographs with relatively low water levels were used.

Data processing and definitions

After visual classification of the planforms, the estuary centrelines and surface areas were automatically determined using GIS software (Figure 3a). The centreline is defined as the mean location line between the polygon boundaries, similar to the approaches of Davies and Woodroffe (2010), Sassi *et al.* (2012) and Kraaijenbrink *et al.* (2016). Subsequently, the centrelines were smoothed with a Polynomial Approximation with Exponential Kernel (PAEK) algorithm in GIS using a tolerance of 0.5 times the maximum channel width. The smoothed line was resampled at an interval of 50 m. At all resampled points, a cross-section was constructed, perpendicular to the centreline and within the boundaries of the channel area (Figure 3a). Smoothing was performed to prevent the direction of cross-sections being highly sensitive to local curves and width variations along the estuary. Now, the width along the centreline of the estuary is given by the length of the successive cross-sections (Figure 3d). The total surface area was obtained by integrating the channel width over distance.

Copyright © 2017 John Wiley & Sons, Ltd.

To assess the quality of our visual classification, the results were compared with the classification of the ecotopes on the geomorphological map of the Western Scheldt (de Jong, 1999; Bouma *et al.*, 2005). The variation and presence of ecotopes along the Western Scheldt estuary in 2012 (Figure 3c) was derived using the same methodology as described above for channel width: for each successive cross-section the total width of each ecotope was calculated. Comparing both approaches (Figure 3d) shows that both methodologies result in similar measurements of active channel width and estuary width, which allows us to extend our visual classification to other estuaries.

It was attempted to digitize up to the tidal limit, but in some cases this was impractical for the PAEK algorithm because of the small size and tight shape of meandering channels at the landward reach of the estuary. For these cases we removed the most landward part of the polygon and defined this area as the offset area (supplementary Table B.1). The polygons were then processed without the offset area to obtain the centreline and channel dimensions. We included the offset area only in the calculation of tidal prisms.

The convergence of estuaries is often measured with the width convergence length or estuary shape factor (Davies and Woodroffe, 2010), which is based on the assumption that estuaries ideally have exponentially converging planforms (Pillsbury, 1956; Langbein, 1963; Savenije, 2006, 2015). The convergence length is the distance over which the channel width of the estuary mouth reduces by a factor e ($\approx$ 2.7), which is calculated as

$$L_W = -s\frac{1}{\ln\left(\frac{W_s}{W_m}\right)} \quad (1)$$

where ln is the natural logarithm, W_m is the width at the estuary mouth, W_s is the width of the estuary at the landward side and s is the distance from W_m to W_s along the centreline of the estuary.

Here we calculate the maximum fitting exponential shape for the active channel planform. We use the mouth width to calculate the convergence length and to fit an exponential function (Figure 5a–c), because a least-squares fit would largely overestimate the width of the mouth in all cases and

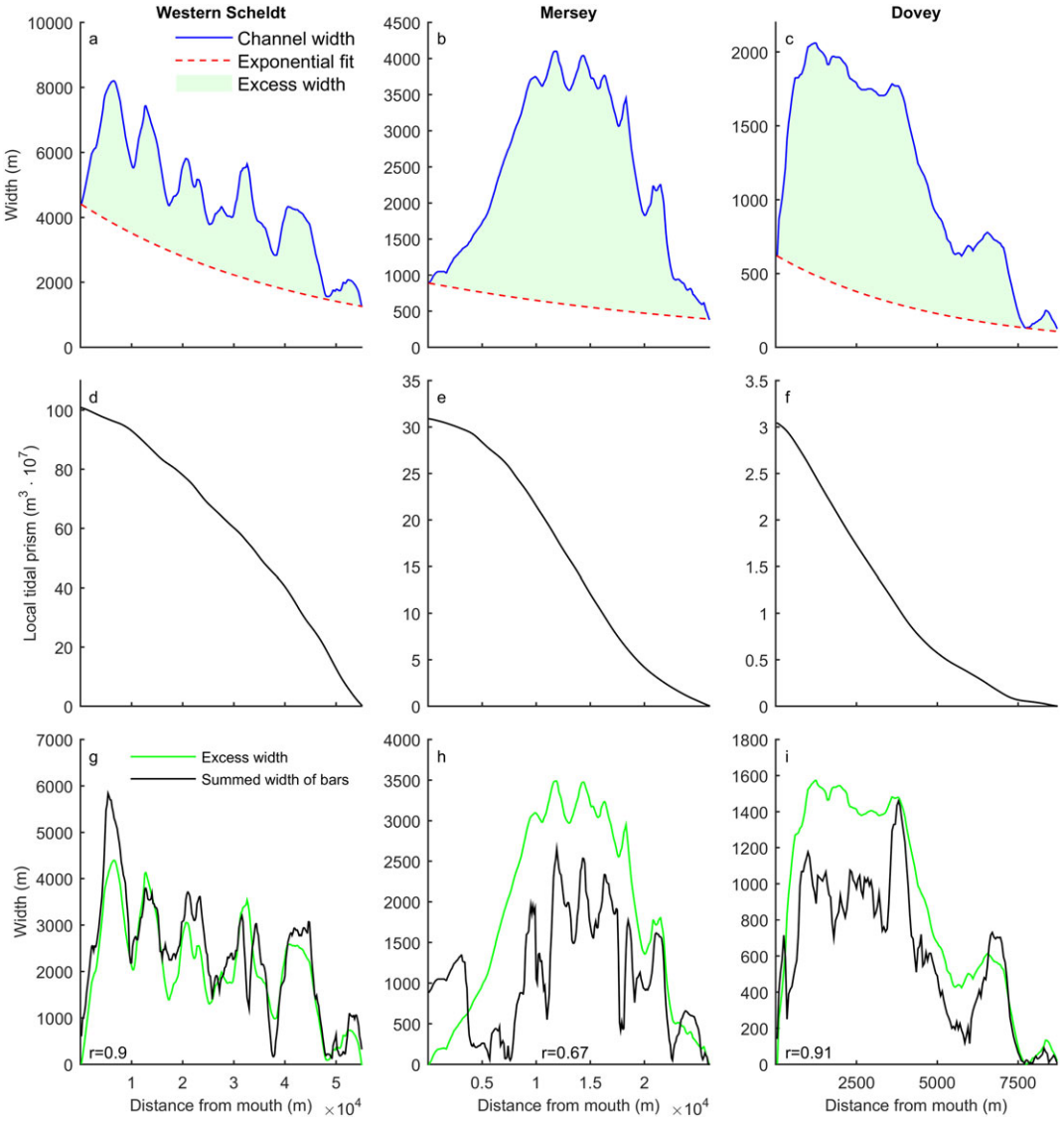

Figure 5. (a, b, c) Channel width along the estuary derived from planform polygons for the three estuaries with bathymetric data (see Figure 1). Exponential functions were fitted onto the width between the mouth and the upstream minimum river width. Excess width was calculated as the channel width minus the exponential fit. (d, e, f) Local tidal prism as estimated from upstream estuary area at mean sea level (MSL) multiplied by tidal range at the mouth. (g, h, i) Comparison between excess width and measured summed width of bars derived from bathymetries. The *r*-values indicate the Pearson product–moment correlation coefficients. [Colour figure can be viewed at wileyonlinelibrary.com]

Copyright © 2017 John Wiley & Sons, Ltd.

therefore also the maximum fitting exponential shape. The resulting fit we used thus depends on the chosen position for the mouth. Since the positioning of the estuary mouth on aerial photographs can be arbitrary, we used the following approach and rationale.

For estuaries in which the mouth was confined by geology, human activity or a higher elevated spit, we selected the location with the minimum width as the position of the mouth (see, for example, Figure 1c, e). In these cases, the minimum mouth width limits the amount of water that can enter the estuary over a tidal cycle. In cases where the mouth was confined with a shallow spit that lacked vegetation or the area around the mouth was widening in the seaward direction, we either chose the location of the mouth at the point where the first tidal flats occur (Figure 1h) or at the location where the beach ends (see, for example, Figure 1a, g).

Savenije (2015) used a similar approach to fit exponential functions for ideal estuaries. Because the ideal estuaries presented by Savenije (2015) typically have a confining inflection point after the mouth of the estuary, two exponential functions were fitted to describe the estuary shape. Moreover, a definition for the position of the mouth was not given there. In contrast to ideal estuaries, the irregular estuary planforms in our dataset are mostly confined at the mouth of the estuary by the presence of a spit or bedrock geology. Therefore, using the minimum width as the location of the mouth in this study is appropriate.

The channel width along the estuary is often larger than the ideal exponential fit (Figure 5a–c), since many alluvial estuaries are confined at their mouth by a spit or due to their antecedent landscape. Here, we define the channel width minus the width of the ideal exponential fit as the excess width (Figure 5a–c). The excess width is generally positive, but may be negative in the case that the channel is constrained by bedrock geology or human interference – for example, the construction of bridges in the Clwyd estuary (UK). We tested the sensitivity of excess width calculations to the measurement of the width of the mouth. A 25% increase or decrease in mouth width affects the calculation of the excess width by a maximum of 10%, but in most cases even less than 5%, since the excess width is often much larger than the exponential channel width.

The aim in this study was to assess how the bar patterns are forced by estuary topography. Part of this forcing may be related to variations in tidal prism. Therefore, the local tidal prism P was approximated as

$$P = 2 \cdot a \cdot A_c \tag{2}$$

in which a is the tidal amplitude, taken as spatially constant (following Savenije, 2006, for ideal estuaries), and A_c is the planform channel area landward of the considered location. Here we used an approach that differs from methodologies that approximate the tidal prism from cross-sectional area (e.g. O'Brien, 1969; Jarrett, 1976; Shigemura, 1980; Eysink, 1990; Friedrichs, 1995; Lanzoni and D'Alpaos, 2015; Gisen and Savenije, 2015) for two reasons. First, the previously proposed relations for tidal systems span an order of magnitude, because most of these relations were only validated for one specific tidal system (supplementary Figure A.12a and supplementary Table B.2). Second, the along-channel variation in bar patterns may not be captured by these relations. After all, the measured along-channel variation in cross-sectional area of non-ideal estuaries – the Western Scheldt, Dovey and Mersey estuaries are used as an example here – can vary such that the cross-sectional area is equal at two locations along the estuary, while the local tidal prism differs by an order of magnitude (Figure 5a–f, supplementary Figure A.12b).

The endpoint of the digitized polygons affects the calculations of tidal prism with Equation (2). The following three factors likely affect the approximation. First, estuaries narrow considerably in the along-channel direction and the contribution of the most landward, narrow part to the tidal prism is thus relatively small. Second, the tidal amplitude decreases upstream, which also limits the contribution of this area to the tidal prism. Last, the displacement of water by tidal wave propagation could cause an overprediction of the tidal prism with Equation (2) in very long estuaries. To assess the quality of our approximation with Equation (2) and the digitized polygons, we compared our approximation with the values reported by Manning (2007).

Manning (2007) approximated the tidal prism with the difference between high water volume and low water volume. The predictions using Equation (2) are, on average, 40% lower than the values of Manning (2007). However, Townend (2005) assessed that the tidal prisms reported by Manning (2007) are, on average, overestimated by 30%, suggesting that our approximation is closer to the real value.

This study focuses on the channel shape in relation to bar pattern. We hypothesize that sediment availability affects this relation for alluvial estuaries, most of which likely formed in the Holocene. To estimate the degree to which an estuary has been filled with sediment based on satellite imagery only, we introduce a fill factor:

$$\text{Fill} = 1 - \frac{A_c}{A_e} \tag{3}$$

in which A_c is the approximate channel area that is active at the present day and A_e is the approximate area of the estuary including mudflats and saltmarshes. The underlying assumption is that the mudflats and saltmarsh are overlying sediment rather than antecedent bedrock.

The summed width of bars was calculated along the channel for three estuaries for which detailed bathymetries were available: the Western Scheldt (NL), Dovey (UK) and Mersey (UK). First, the same methodology was used as for the data collection of channel planform (see previous subsection). Second, bathymetric profiles with bed elevation were extracted at the cross-sections to determine the summed width of bars. To do so, the median bed elevation was determined for each cross-section. Subsequently, a linear and an exponential regression were fitted for median bed elevation along the estuary channel (supplementary Figure A.13). Summed width of bars was determined as the total width of the estuary above this regression line. In addition, the summed width of bars was determined as the total width above the mean low water surface plane (supplementary Figure A.13). Supplementary Figure A.14 (supporting information) shows the sensitivity of our results to the threshold for bar recognition in bathymetry. Dependent on the type of tidal system (e.g. tidal creeks or estuaries) and along-channel width profile (e.g. constant width or converging), varying approximations were found for the along-channel bed profile, such as concave, linear and horizontal (Savenije, 2006; Toffolon and Lanzoni, 2010; Savenije, 2015). Since the estuary depth profile often shows a linear or almost linear profile (Savenije, 2015), the linear threshold is used here to calculate the summed width of bars in the remainder of this paper (supplementary Figure A.14).

Since bathymetry is available for three estuaries, we will first describe how tidal bars are forced by topography for these three cases. Then, we assess the uncertainty in the along-channel bar pattern as obtained from our automated approach for bathymetries. Subsequently, we compare the definitions used in the automated approach for bathymetries with

Copyright © 2017 John Wiley & Sons, Ltd.

the definitions used in a geomorphological map of the Western Scheldt estuary. Last, the results from point observations on aerial photographs of 35 estuaries are compared with the results for the three detailed cases. This will allow testing our hypotheses against a larger database with estuaries.

The larger dataset with point measurements was also used to obtain linear regressions for the hydraulic geometry of estuarine channels and relations for individual bar width as a function of channel width or tidal prism.

In all cases where statistical analyses are presented, the following approach was used. For linear regressions, the residuals were minimized in both the x- and y-directions because this is more robust and conservative than either one of the two. Where regressions are plotted, confidence limits are given for two standard deviations from the regression. For the confidence limits, the legends show the approximate multiplication factor that the confidence limits plot higher or lower than the trend and the R^2 value, which gives the variance around a regression. The quality of all along-channel predictors for bar pattern was assessed with the r-value (Pearson product–moment correlation coefficient), which is a measure of both the direction and strength of a correlation.

Results

In this section, we first show how the location of tidal sand bar formation is controlled by the topography. Second, a relation between channel width and tidal prism is presented based on data from 35 estuaries. We assess how this relation is influenced when estuaries deviate from the ideal converging planform and compare the results with previous studies. Lastly, we present empirical rules of thumb to predict bar dimensions, which are subsequently used to predict braiding index.

The locations where bars form

The along-channel variation in summed width of bars correlates well with the excess width for the Western Scheldt and Dovey ($r > 0.9$) (Figure 5g, h, i). This shows that tidal sandbars typically form at locations where the channel is wider than an ideal exponential shape. Moreover, excess width is within a factor of 1.25 of the total width of bars at most locations. Following convention this means that most excess widths are only 1.25 times larger or smaller than the summed width of bars.

The correlation between excess width and summed width of bars is dependent on the threshold that was chosen for bar recognition in bathymetries. This can explain why the correlation for the Mersey is lower ($r = 0.67$) than for the Dovey and Western Scheldt. A linear fit was used on the median bed elevation to recognize bars, because most estuaries have a linearly increasing bed profile (Savenije, 2015, Braat *et al.*, 2017). Moreover, long-term morphological models also showed the evolution of linear bed profiles in estuaries with and without mud (Braat *et al.*, 2017). In our results, the Mercey forms an exception, because it has an exponential bed profile. In this case, fitting a linear threshold on the median bed elevation will result in a threshold that is too low at the mouth of the estuary and too high for the remainder of the estuary. This causes a measurement of the summed width of bars that is too large for the first 4 km from the mouth and too small for the remainder of the estuary. After all, the first 4 km lack tidal bars (Figure 1f). If an exponential fit would have been adopted for the Mersey, the correlation between excess width and summed width of bars would increase to a value of $r = 0.91$ (supplementary Figure A.14b). This implies that the method to determine the threshold for bar recognition should be adapted to the shape of the bed profile, for estuaries that deviate from a linear bed profile. At present, we lack knowledge on the evolution of bed profiles and equilibrium bed profiles in natural estuaries. We urge the need to study this evolution and to test what equilibrium bed profiles evolve in experiments, models and natural systems. In all other estuaries for which point measurements were made of the summed width of bars, it was measured from aerial photographs. Therefore, the point measurements of summed width of bars presented hereafter are independent of a threshold in bed level as used for the bathymetries.

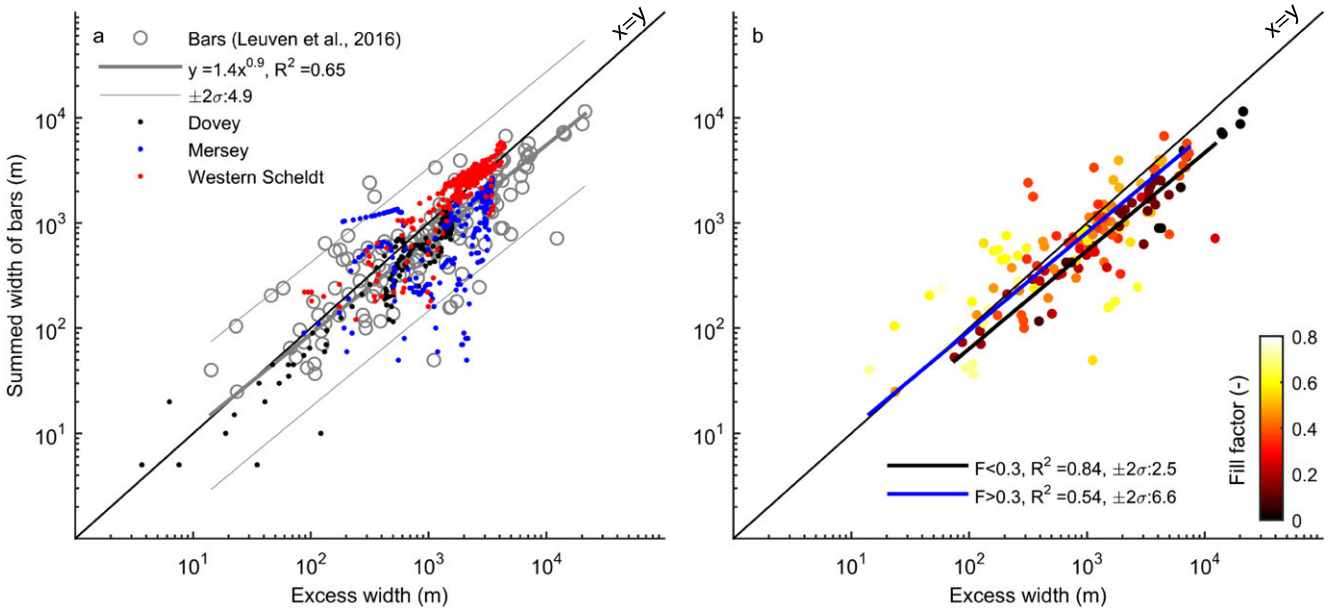

Figure 6. (a) Relation between summed width of bars and excess width at bar locations for all estuaries. In addition, the along-channel variation in the Western Scheldt, Mersey and Dovey is shown, which shows similar scatter as the full dataset. Confidence limits are given for two standard deviations from the regression. The approximate multiplication factor that the confidence limits plot higher or lower than the trend is given in the legend. Summed width of bars approaches excess width as can be seen from the scatter around the line of equality. (b) Same, colour-coded with a proxy for the fraction of sediment infill (Equation (3), see text for explanation). [Colour figure can be viewed at wileyonlinelibrary.com]

Copyright © 2017 John Wiley & Sons, Ltd.

A comparison of the geomorphological map of the Western Scheldt with our polygons of estuary area and active channel area shows that the definitions of channel width and estuary width are very similar (Figure 3d). Moreover, it shows that the width of low dynamic environments is generally higher at locations where summed width of bars is higher and lower at locations where summed width of bars is smaller (correlation of $r = 0.6$). This shows that ecologically valuable low dynamic environments (Meininger *et al.*, 2003; van Eck and Holzhauer, 2007; Cleveringa, 2007) form at similar locations where bars form, namely the locations with excess width.

The 35 estuaries show similar results as the three detailed cases: summed width of bars increases with excess width (Figure 6a). The scatter significantly increased and the goodness of fit decreased when the excess width was calculated using other definitions, such as fitting an exponential function to the maximum and minimum channel width or using a least-squares fit (e.g. $R^2 = 0.1$ and $2\sigma = 21$).

Figure 6a shows that the along-channel variation for the three detailed cases varies within the same range as the local measurements in 35 estuaries. In Leuven *et al.* (2016) we found that the effect of unknown water level and tidal phase is a factor of 2 uncertainty in measured bar dimensions. The uncertainty in measurement of summed width of bars in bathymetry is also approximately a factor 2 compared to the mean measured value, which arises from the threshold definition for bar recognition (supplementary Figure A.14). The remaining scatter is perhaps due to disequilibrium between the bar pattern and channel geometry.

We estimated the amount of sediment received (Equation (3)), because we hypothesized that insufficient sediment supply would reduce the formation of bars and therefore the summed width of bars too. We found that the summed width of bars is, on average, larger for estuaries that received relatively more sediment (Fill > 0.3) compared to systems that received relatively little sediment (Fill < 0.3) (Figure 6b). Moreover, only the summed width of bars in filled estuaries exceeds the excess width in some cases, which is illustrated by the points that exceed the line of equality in Figure 6b. This suggests that unfilled estuaries have less bar development. Nevertheless, a regression on the subsets of the data show that the difference between the regressions is insignificant, because their confidence limits would largely overlap. Therefore, we abstain here from a relation between the infilling and the extent to which the summed width of bars approaches the excess width.

Hydraulic geometry

The dimensions of individual bars relate to channel width (Leuven *et al.*, 2016) and the summed width of bars correlates with excess width. This means that, to predict bar pattern, channel width and excess width should be predicted first. Using hydraulic geometry, the channel width could be calculated with discharge or tidal prism. Many relations were proposed in the past for hydraulic geometry of rivers and tidal systems (Lacey, 1930; Leopold and Maddock, 1953; Langbein, 1963; Hey and Thorne, 1986; Savenije, 2003; Sassi *et al.*, 2012; Gisen and Savenije, 2015) (supplementary Table B.2). However, there are two issues in applying these relations to tidal systems. First, many of the relations consider either ideal systems or describe only the mouth of tidal systems, while to study bar pattern the along-channel width is required. Second, two points on an irregular channel can have an equal channel width but have different local tidal prisms because the geometry upstream differs (e.g. Figure 5a–f). Channel depth can partly compensate for this, but we found also that for two sections with the same cross-sectional area two different tidal prisms can occur (supplementary Figure A.12).

The dataset with measurement points in 35 estuaries shows that, despite the irregularities in channel planform, a simple relation exists between the channel width and local tidal prism (Figure 7a):

$$W = 0.05 \cdot P^{0.59} \tag{4}$$

In Figure 7b, the along-channel variation of hydraulic geometry in the Western Scheldt, Mersey, Dovey and the regression

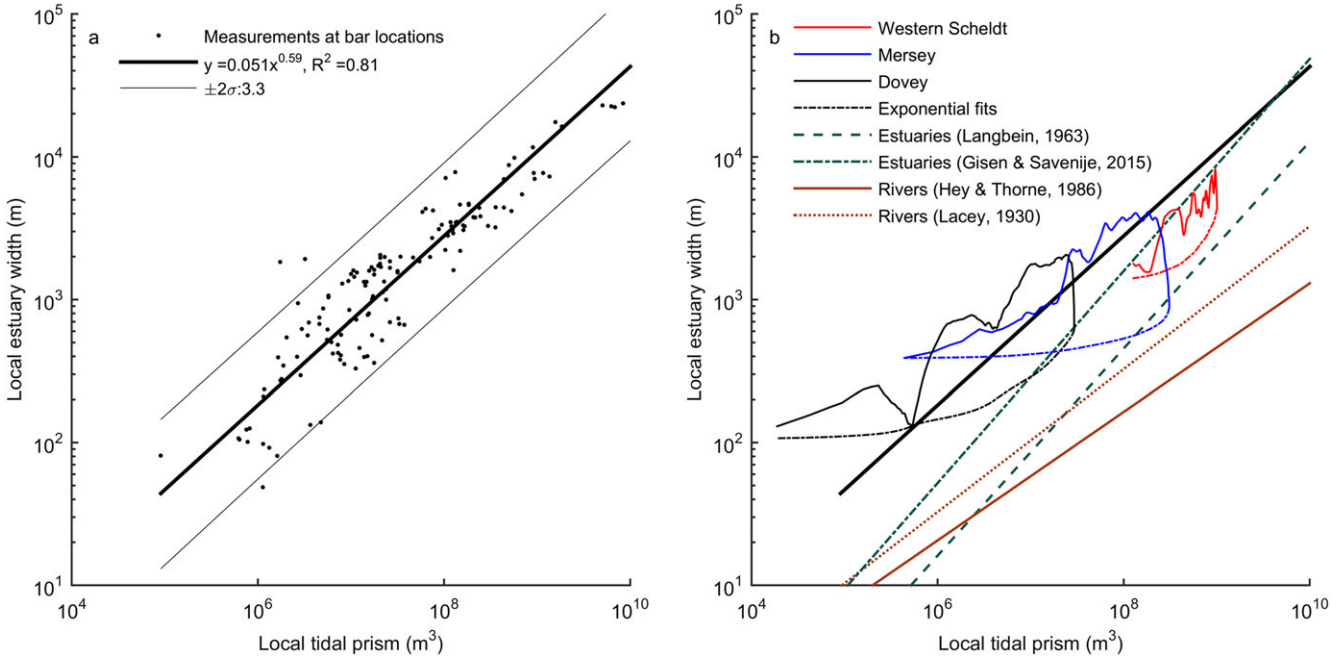

Figure 7. Active channel geometry related to tidal flow. (a) Channel width as a function of local tidal prism for 35 estuaries. (b) Along-channel measurements of channel width for the Western Scheldt, Mersey and Dovey. For comparison, representative hydraulic geometry relations for estuaries and rivers are drawn (see Supplementary Figure A.12 and Supplementary Table B.2 for overview of most relations from the literature between tidal prism and cross-sectional area.). [Colour figure can be viewed at wileyonlinelibrary.com]

Copyright © 2017 John Wiley & Sons, Ltd.

from the dataset are compared with point measurements and hydraulic geometry relations. The along-channel variation is of the same magnitude as the scatter in the dataset and illustrates that a certain width may be found with different tidal prisms, depending on the amount of excess width at that location. The exponential fits for these three cases are similar to the relations proposed by Langbein (1963) for ideal estuaries and Gisen and Savenije (2015), who predicted channel width based on the upstream bankfull river discharge and a typical estuary convergence length.

The general finding that width increases with tidal prism and with discharge is in agreement with studies in other environments such as rivers, deltas and tidal creeks (Lacey, 1930; Leopold and Maddock, 1953; Langbein, 1963; Hey and Thorne, 1986; Savenije, 2003; Sassi et al., 2012; Gisen and Savenije, 2015; Lanzoni and D'Alpaos, 2015). However, deviations from ideal estuaries (Langbein, 1963; Gisen and Savenije, 2015) or rivers (Lacey, 1930; Leopold and Maddock, 1953; Hey and Thorne, 1986; Savenije, 2003) are present: (i) no significant relations were found between estuary depth and tidal prism, which shows in the wider scatter in supplementary Figure A.12b than in Figure 7a; (ii) non-ideal estuaries are generally wider and have larger cross-sectional areas than rivers and ideal estuaries under equal discharge (supplementary Figure A.12b), because their width is typically equal to the sum of the ideal width and the excess width, which is determined by the antecedent topography that was present before Holocene transgression.

Effect of channel planform on bar pattern

The bar pattern, i.e. bar shape, length and width, in estuaries is a result of its channel planform. It was illustrated above that the bar location and the summed bar width were predicted by the excess width. In this section, we present a predictive braiding index that indicates how many channels and bars are likely to be present at a given location. The predicted braiding index (BI) is as follows:

$$\mathrm{BI} = \frac{W_{\mathrm{excess}}}{w} \tag{5}$$

where W_{excess} is the excess width and w is a predicted bar width (explained later, Equations (6)–(9)). Because two different measures can be used for w, namely the partitioned bar width (w_p) and the average bar width (w_{avg}), we will first discuss the definition of these measures and of the braiding index before the relations for bar width are presented. Partitioned bars are those that are separated by the number of barb channels. Leuven *et al.* (2016) identified that after partitioning all bars can be described by an elongated shape for which the bar length is approximately seven times the bar width.

The braiding index is highly sensitive to water-level variations (Leuven *et al.*, 2016) and thus also to the threshold between channel and bar recognition from the bathymetries. Applying the partitioned bar width to predict the braiding index would give the sum of channels and barb channels, meaning it will overpredict the braiding index. Therefore, we used the average bar width rather than the partitioned bar

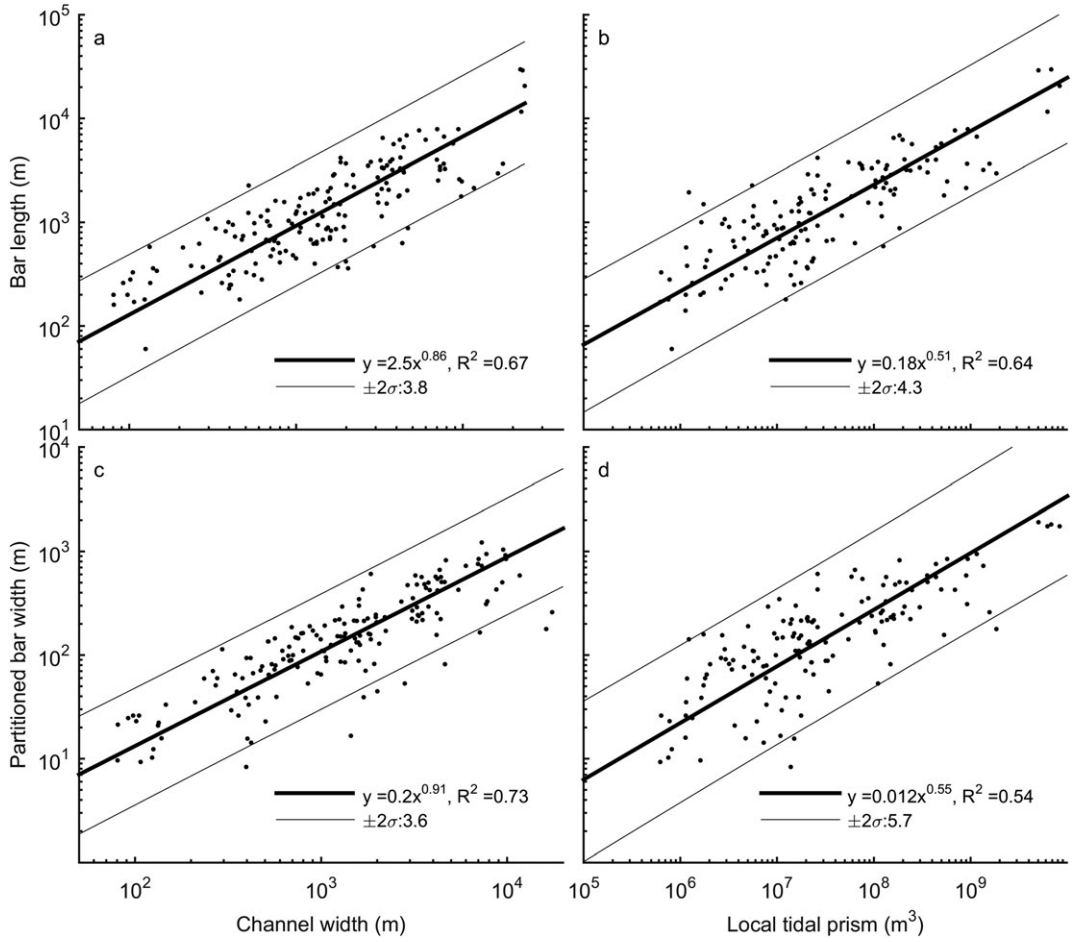

Figure 8. Individual bar dimensions related to channel width and local tidal prism. Bar length and width increase with channel width (a, c) and local tidal prism (b, d). Confidence limits are given for two standard deviations from the regression. The approximate multiplication factor that the confidence limits plot higher or lower than the trend is given in the legend.

Copyright © 2017 John Wiley & Sons, Ltd.

width. To record the braiding index from bathymetries, we used a linear fit on the median bed elevation first to distinguish bars (above the fitted median bed elevation) from channels (below the fitted median bed elevation) and subsequently calculated the braiding index from the number of channels. Using this approach, the shallower barb channels are part of the bar and not accounted for in the braiding index. Given this definition of channels and bars we calculated the average bar width to predict the braiding index. Bar length and bar width depend on local channel width (W) and become longer and wider for increasing W. Analysis of our dataset on channel width for both the partitioned bar width and the average bar width (Figure 8) resulted in a new empirical relation for the partitioned bar width (w), which is

$$w_{p,W} = 0.20 \cdot W^{0.91} \tag{6}$$

and, alternatively with local tidal prism (P):

$$w_{p,P} = 0.012 \cdot P^{0.55} \tag{7}$$

where $w_{p,W}$ is the partitioned bar width predicted with local channel width (W) and $w_{p,P}$ is the partitioned bar width predicted with tidal prism. All relations are valid over at least two orders of magnitude. These relations allow prediction of the dimensions of individual bars based on solely the channel width, or on the upstream channel planform area and tidal range. The goodness of fit is higher for predictions from channel width than as a function of local tidal prism.

The empirical relations for average bar width (w_{avg}) are

$$w_{avg,W} = 0.39 \cdot W^{0.92} \tag{8}$$

or

$$w_{avg,P} = 0.022 \cdot P^{0.55} \tag{9}$$

Obviously, these relations simplify barbs, channels and bars as discrete elements in a continuous field of bed elevations. Over time, barbs may develop into channels and vice versa, which illustrates the need for a better understanding of formative mechanisms, dynamics and development of the barb channels, which is beyond the scope of this paper.

Figure 9d–f shows the predicted braiding index using Equation (5) with either bar width predictions based on the channel width or the local tidal prism. Best predictions are obtained when channel width is used, with correlation coefficients all above 0.62. Predictions for braiding index are all within a factor of 2 of the measured value, but generally better. Using the local tidal prism to predict braiding index may result in large overpredictions at the landward part of the estuary (for example, for the Dovey, Figure 9f) or underpredictions at the seaward side (for example, for the Mersey, Figure 9e).

At the landward boundary, the local tidal prism approaches zero. As the local tidal prism lowers, the predicted bar width also decreases. However, some landward locations may have a relatively large local channel width and excess width. In these cases, dividing the excess width by a very small bar width, the prediction of braiding index will be very high. At the seaward boundary, the same reasoning causes an underprediction of the braiding index. In summary, using the tidal prism one would predict a gradual decrease in bar width that lacks any dependency on channel width and transfers to predictions of braiding index, because it is predicted as the excess width divided by the predicted bar width. In this case, the predictions of braiding index are thus too sensitive to local variations in channel width, where in natural systems the bar width adapts to the varying channel size.

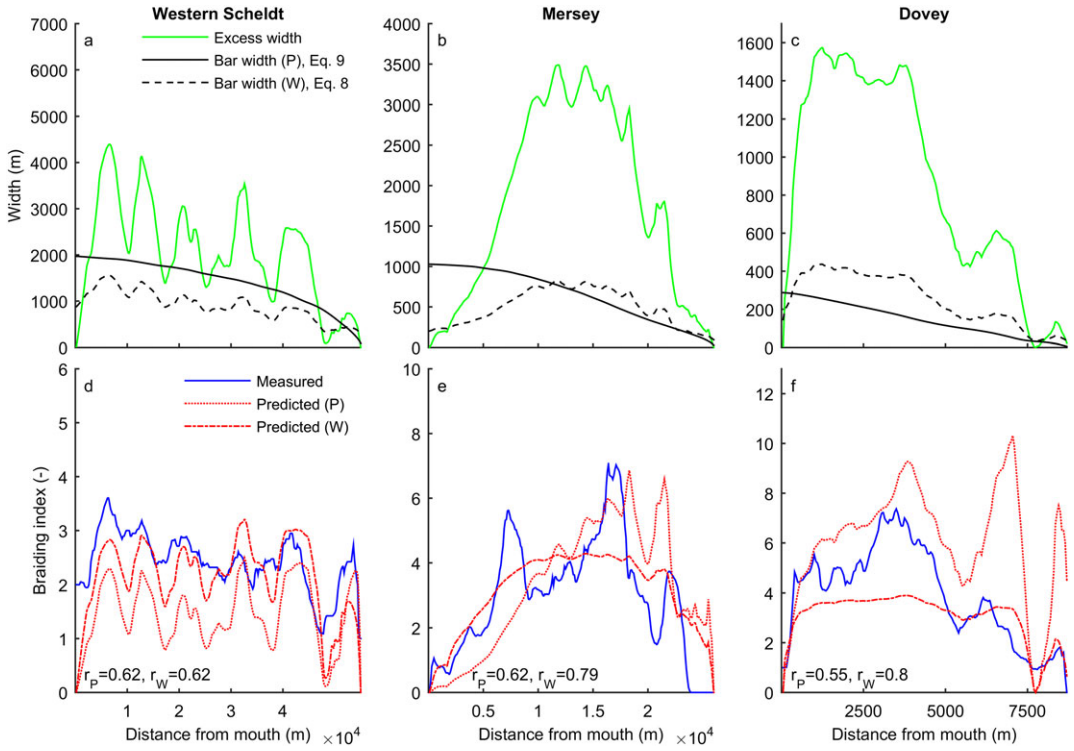

Figure 9. (a, b, c) The along-channel excess width and prediction of bar width using the empirical relations with tidal prism (P, Equation (9)) and channel width (W, Equation (8)) for the three estuaries with bathymetric data. (d, e, f) Predicted and measured braiding index. Predicted braiding index was calculated as excess width divided by predicted bar width. The r-values indicate the Pearson product–moment correlation coefficients for measured and predicted braiding index, where subscripts indicate whether bar width was predicted with tidal prism (P) or channel width (W). [Colour figure can be viewed at wileyonlinelibrary.com]

Copyright © 2017 John Wiley & Sons, Ltd.

Discussion

We first summarize how bar pattern is forced by channel planform and discuss why excess width is a measure required to predict bar pattern. Second, the empirical predictions are compared with theoretical predictions from stability analysis of Schramkowski *et al.* (2002). Last, we discuss the long-term evolution of bar patterns and estuarine filling.

Forcing of bar pattern by planform

Tidal sandbars form at locations where the estuary is wider than an ideal exponential fit (Figure 5). Here, local flow expansion occurs due to the presence of embayments that were inherited from the antecedent landscape. The local flow expansion results in a reduction of stream velocity and shear stress, which can cause sedimentation when sufficient sediment is available (Cant and Walker, 1978; Ashmore, 1991; Ashworth *et al.*, 2000). In filled estuaries, summed width of bars approximates excess width for most estuaries (Figure 6a). In contrast, unfilled estuaries can have a lower summed width of bars, being around 50% of the excess width (Figure 6b).

At the location where bars form, the individual dimensions of bars scale particularly well with channel width (Figure 8a, c). Although local tidal prism could be used, predictions from channel width are better fits and tidal prism is more difficult to measure. In agreement with our hypothesis, bar dimensions are poorly predicted from ideal channel width. The result that bar dimensions are determined by local channel geometry raises the question of what sets the size and shape of an estuarine channel and how it evolves over time. Many estuaries formed during the early to middle Holocene when valleys drowned during rapid sea-level rise (e.g. van der Spek and Beets, 1992; Hijma and Cohen, 2011). Because of a progressively decelerating sea-level rise, sediment input in many of these systems eventually exceeded creation of accommodation space by sea-level rise, resulting in progressive infilling of these estuaries. The present-day estuary shape is thus the sum of the initial valley size and shape as well as historical creation of accommodation space and infilling, and varies between estuaries.

The measure of excess width is required to explain the variation in bar pattern for two locations with equal channel width along the same estuary. It is a priori known that the seaward location is affected by a larger tidal prism than the landward location. According to hydraulic geometry (Equation (4), supplementary Figure A.12), a larger cross-sectional channel area is expected at the seaward location. Given that the prediction of individual bar width is equal at both locations, this also implies that the seaward location has a lower excess width and therefore a smaller summed width of bars and a lower braiding index. Therefore, multiple braiding indices and summed width of bars could occur for the same channel width (Figure 10b, d).

Alternatively, let us consider two locations with equal summed width of bars or equal braiding index. Following the same reasoning, there can be multiple locations along the estuary where either an equal summed width of bars or braiding index occurs. Each of these locations is characterized by a different local tidal prism, which explains that for each braiding index or summed width of bars a wide range of local tidal prisms can occur. This explains the wide horizontal scatter in Figure 10a, c. We therefore conclude that a measurement of local tidal prism or local channel width is insufficient to predict bar pattern and that a measurement of the excess width is required to obtain more accurate predictions of braiding index and summed width of bars.

Comparison with theory

The theoretical approach to predict bar pattern differs from the empirical approach in this study. Previous studies attempted to predict bar pattern in estuaries using linear stability analyses (Seminara and Tubino, 2001; Schramkowski *et al.*, 2002; see Leuven *et al.*, 2016, for a review). We applied the theory of Schramkowski *et al.* (2002) using the along-channel width profile and the average channel depth of three estuaries. For the remaining parameters the default values given in Leuven *et al.* (2016) were used. Predictions from theory show similar trends to the new empirical predictors (Figure 11), probably because excess width is partly a surrogate of the width-to-depth ratio that was found to control braiding index in theory. However, the theoretical results are very sensitive to input parameters such as bed slope effect and friction (Leuven *et al.*, 2016). Moreover, theory underestimates the effect of estuary dimensions and, in particular, channel width. For example, theoretical predictions overpredict braiding index consequently by a factor of 2 for the Western Scheldt (Figure 11a), while braiding index in the Dovey is underestimated by at least a factor of 2 (Figure 11c).

Theory also consistently mispredicts the summed width of bars, which is underpredicted where the excess width is large (Figure 11d–f) and overpredicted where the estuary is narrow and close to the ideal width. The reason is that bars in the bar theory are regarded as cosine waveforms that are, on average, symmetrical about the horizontal. Therefore, we assume that theory will always predict the summed width of bars to be approximately 50% of the channel width (Figure 11d–f), independent of channel width and excess width, and thus also for locations where the channel is too narrow to accommodate bars. Minor deviations from the 50% approximation may occur for very small braiding indices (Fujita, 1989). Nevertheless, the predicted braiding index is generally well above 1 for the estuaries considered in this study (Figure 11a–c), which justifies this assumption.

Potential applications of empirical bar predictors

Our empirical method predicts the summed width of bars that are accurate within a factor of 1.25 and the braiding index accurate within a factor of 2. This insight can be implemented in several types of geological reconstructions where tidal channel belts or estuary shapes may have been identified, but wherein infilling and bar configuration are unknown. On the one hand, the bar pattern within tidal channel belts affects lithological properties of the geological channel body (Wood, 2004), such as the connectivity and permeability that influence storage capacity. On the other hand, our empirical approach may successfully estimate bar pattern for palaeogeographical reconstructions (Vos *et al.*, 2015; Pierik *et al.*, 2016) of former estuaries where the morphology of bars is typically not recognizable in the geological record. This exercise may be especially relevant for bar-built, high-stand estuaries which are sufficiently filled with sediment, such that the bar pattern has been developed. Estimating bar properties will improve the palaeogeographical maps, because it allows us to estimate the location and number of tidal bars, based on the outline of the palaeo-estuary. It further enables reconstructing past water levels or tidal wave

Copyright © 2017 John Wiley & Sons, Ltd.

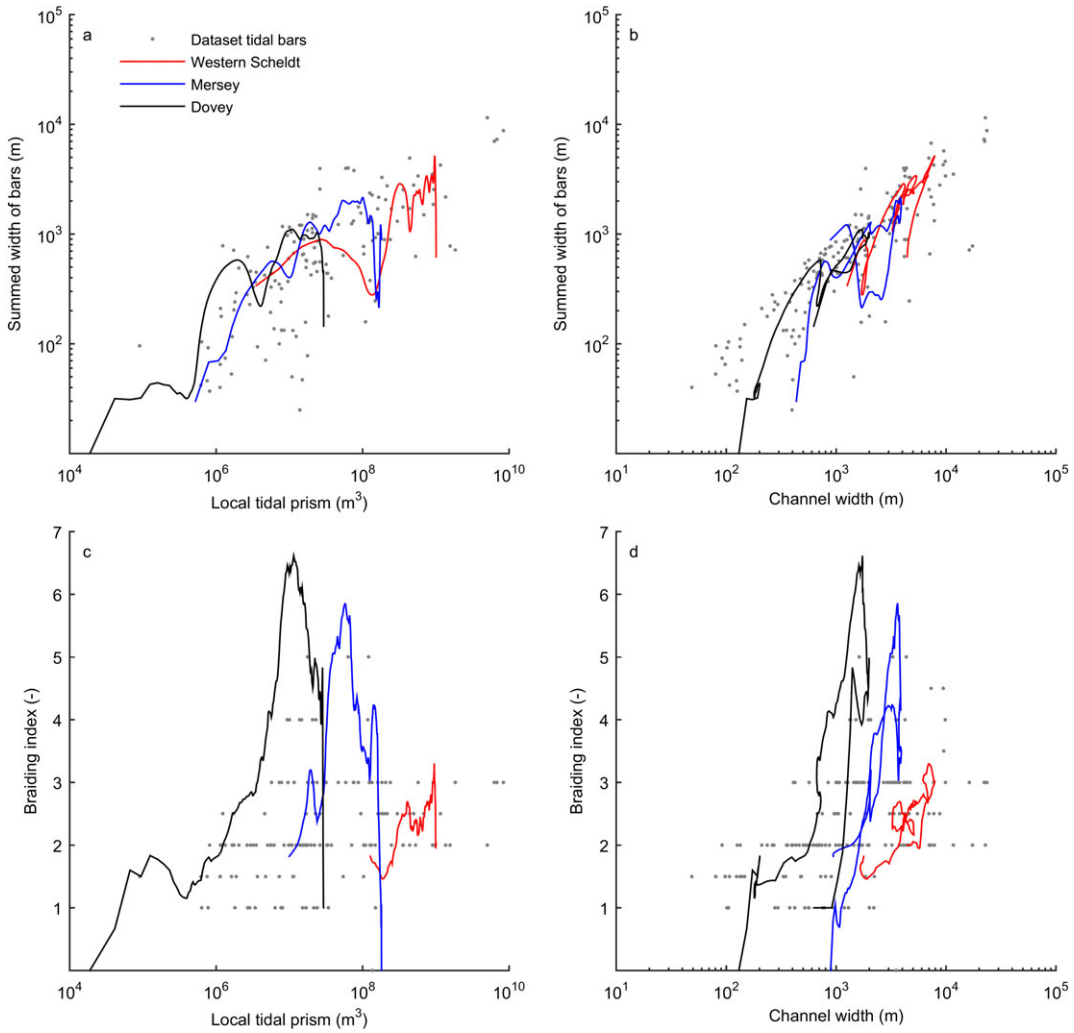

Figure 10. Summed width of bars as a function of local tidal prism (a) and channel width (b). Measured braiding index as a function of local tidal prism (c) and channel width (d). The along-channel variation in summed width of bars and braiding index along a single estuary is similar to the scatter within the dataset of 170 tidal bars in 35 estuaries. [Colour figure can be viewed at wileyonlinelibrary.com]

propagation, and therefore may improve understanding of the evolution of the estuary. The quality of our empirical predictions is generally better than the theoretical predictions (Seminara and Tubino, 2001; Schramkowski *et al.*, 2002) and only requires channel planform measurements. While the understanding gained from empirically valid theories is valuable, further theory development is urgently needed.

Given time, tidal sandbars may stabilize by means of vegetation succession (Gray, 1992, Thomson *et al.*, 2004, van der Wal *et al.*, 2008), finally resulting in supratidal flats that are no longer morphologically active in common tidal conditions (van den Berg *et al.*, 1996; Cleveringa, 2007). This raises the question to what degree tidal bars are stable in time and space after they have formed. The methods presented herein can now be applied to reconstructed Holocene estuaries (Vos *et al.*, 2015; Pierik *et al.*, 2016), for which boundaries are well known but bars are usually not preserved, as well as estuaries in numerical models and laboratory experiments (Kleinhans *et al.*, 2015). This will allow us to systematically study the effects of boundary conditions and vegetation on the dynamics of tidal bars over time and on the evolution of the entire estuary from initiation on inherited landscapes.

We found typical relations between tidal bar dimensions, tidal prism and channel width (Figure 8). Using the empirical relations for bar dimensions as a function of estuary dimensions also allows a reverse approach. With single measurements of bar dimensions it would be possible to reconstruct the local tidal prism and width. The architecture of tidal bars in the geological record can possibly be used to obtain predictions of the hydraulic geometry of the corresponding estuary within a factor 3 accuracy.

Conclusions

Here we empirically studied effects of channel planform on tidal bar patterns in estuaries with a newly collected dataset of sandbar dimensions and channel planforms of non-ideal alluvial estuaries. We found that simple empirical relations adequately describe bar dimensions and braiding index. Sandbars mainly form where the estuary is wider than expected from an ideal exponentially converging planform between the mouth and the upstream river. At these locations, local flow expansion causes a reduction of the shear stress, which can result in the deposition of sediment. The summed width of bars approximates the excess width over time, reducing the channel width to the ideal channel width. Bars are narrower when sediment is less abundant. Since channel width and local tidal prism are strongly related, the dimensions of individual bars can be predicted from either of these quantities, but the quality of predictions is highest when channel width is used. Dividing the excess width by the bar width resulted in predictions for braiding index, which were accurate within a factor of 2. Our results imply that present estuary planform

Copyright © 2017 John Wiley & Sons, Ltd.

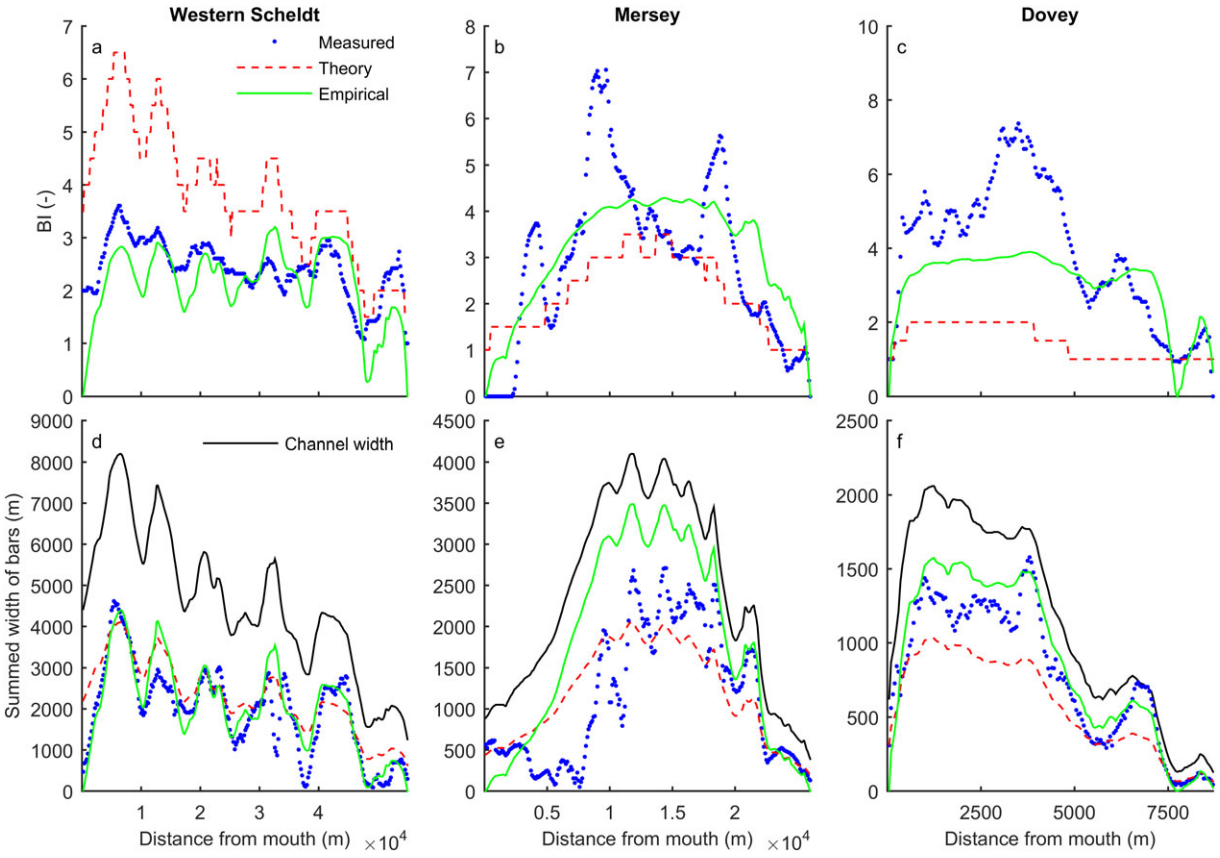

Figure 11. Comparison between braiding index (a, b, c) and summed width of bars (d, e, f) predicted by theory of Schramkowski *et al.* (2002) and predicted from empirical relations for the three estuaries with bathymetric data. Braiding index was calculated as the excess width divided by the bar width, as predicted from Equations (5) and (8). [Colour figure can be viewed at wileyonlinelibrary.com]

shape, including mudflats and saltmarsh, depends on inherited Holocene topography, but that eventually convergent channels will form when sufficient time and sediment are available. The simple relations between bar pattern and local estuarine channel width may aid predictions of the architecture of tidal bar deposits and palaeogeographical reconstructions of former estuaries.

Acknowledgements— This research was supported by the Dutch Technology Foundation TTW (grant Vici 016.140.316/13710 to MGK, which is part of the Netherlands Organisation for Scientific Research (NWO), and is partly funded by the Ministry of Economic Affairs). This work is part of the PhD research of JRFWL and LB. We are grateful to Maarten Zeylmans van Emmichoven and Philip Kraaijenbrink for their support with GIS. Discussions with Maarten van der Vegt, Willem-Bart Bartels, Lex Dolfing, Harm Jan Pierik, Janrik van den Berg and Wout van Dijk are acknowledged for discussion during this project. Reviews by two anonymous reviewers and steer by the Associate Editor helped to improve the manuscript. The authors contributed in the following proportions to conception and design, data collection, analysis and conclusions, and manuscript preparation: JRFWL (65, 95, 85, 80%), TdH (15, 5, 5, 5%), LB (5, 0, 0, 5%), MGK(15, 0, 10, 10%).

References

Ashmore PE. 1991. How do gravel-bed rivers braid? *Canadian Journal of Earth Sciences* **28**(3): 326–341.

Ashworth PJ, Best JL, Roden JE, Bristow CS, Klaassen GJ. 2000. Morphological evolution and dynamics of a large, sand braid-bar, Jamuna River, Bangladesh. *Sedimentology* **47**(3): 533–555.

Bouma H, de Jong D, Twisk F, Wolfstein K. A Dutch ecotope system for coastal waters (zes. 1), to map the potential occurrence of ecological communities in Dutch coastal and transitional waters, Technical Report RIKZ/2005.024, Rijkswaterstaat, 2005.

Braat L, van Kessel T, Leuven JRFW, Kleinhans MG. 2017. Effects of mud supply on large-scale estuary morphology and development over centuries to millennia. *Earth Surface Dynamics Discussions* **2017**: 1–47.

Cant DJ, Walker RG. 1978. Fluvial processes and facies sequences in the sandy braided south Saskatchewan River, Canada. *Sedimentology* **25**(5): 625–648.

Cleveringa J. 2007. Milieueffectrapport verruiming vaargeul beneden-zeeschelde en Wester-Schelde. 070622 Versie 4.1, Consortium ARCADIS – Technum.

Crosato A, Mosselman E. 2009. Simple physics-based predictor for the number of river bars and the transition between meandering and braiding. *Water Resources Research* **45**(3): 1–14 W03424.

Dalrymple RW, Choi K. 2007. Morphologic and facies trends through the fluvial–marine transition in tide-dominated depositional systems: a schematic framework for environmental and sequence-stratigraphic interpretation. *Earth-Science Reviews* **81**(3): 135–174.

Davies G, Woodroffe CD. 2010. Tidal estuary width convergence: theory and form in North Australian estuaries. *Earth Surface Processes and Landforms* **35**(7): 737–749.

de Jong D. Ecotopes in the Dutch marine tidal waters: a proposal for a classification of ecotopes and a method to map them, Technical Report RIKZ-Report 99.017, Rijkswaterstaat, 1999.

Eysink W. 1990. Morphologic response of tidal basins to changes. *Coastal Engineering Proceedings* **1**(22): 1948–1961.

Friedrichs CT. 1995. Stability shear stress and equilibrium cross-sectional geometry of sheltered tidal channels. *Journal of Coastal Research* **11**(4): 1062–1074.

Friedrichs CT, Aubrey DG. 1994. Tidal propagation in strongly convergent channels. *Journal of Geophysical Research* **99**: 3321–3321.

Fujita Y. 1989. Bar and channel formation in braided streams. In *River Meandering*, Ikeda S, Parker G (eds), American Geophysical Union: Washington, DC; 417–462.

Copyright © 2017 John Wiley & Sons, Ltd.

Gisen JIA, Savenije HH. 2015. Estimating bankfull discharge and depth in ungauged estuaries. *Water Resources Research* **51**(4): 2298–2316.

Gray AJ. 1992. Saltmarshes: morphodynamics, conservation and engineering significance. In *Saltmarshes: Morphodynamics, Conservation and Engineering Significance*, Allen J, Pye K (eds), Cambridge University Press: Cambridge, UK; 63–79.

Hey RD, Thorne CR. 1986. Stable channels with mobile gravel beds. *Journal of Hydraulic Engineering* **112**(8): 671–689.

Hijma MP, Cohen KM. 2011. Holocene transgression of the Rhine river mouth area, The Netherlands/southern North Sea: palaeogeography and sequence stratigraphy. *Sedimentology* **58**(6): 1453–1485.

Jarrett JT. Tidal prism–inlet area relationships, Technical Report WES-GITI-3, DTIC Fort Belvoir, VA, 1976.

Kleinhans MG, Scheltinga RT, Vegt M, Markies H. 2015. Turning the tide: growth and dynamics of a tidal basin and inlet in experiments. *Journal of Geophysical Research: Earth Surface* **120**(1): 95–119.

Kleinhans MG, van den Berg JH. 2011. River channel and bar patterns explained and predicted by an empirical and a physics-based method. *Earth Surface Processes and Landforms* **36**(6): 721–738.

Kraaijenbrink P, Shea J, Pellicciotti F, de Jong S, Immerzeel W. 2016. Object-based analysis of unmanned aerial vehicle imagery to map and characterise surface features on a debris-covered glacier. *Remote Sensing of Environment* **186**: 581–595.

Lacey G. 1930. Stable channels in alluvium. In *Minutes of the Proceedings of the Institution of Civil Engineers*, Vol. 229, Thomas Telford–ICE Virtual Library: London; 259–292.

Langbein W. 1963. The hydraulic geometry of a shallow estuary. *Hydrological Sciences Journal* **8**(3): 84–94.

Lanzoni S, D'Alpaos A. 2015. On funneling of tidal channels. *Journal of Geophysical Research: Earth Surface* **120**(3): 433–452.

Lanzoni S, Seminara G. 1998. On tide propagation in convergent estuaries. *Journal of Geophysical Research* **103**: 30793–30812.

Leopold LB, Maddock T Jr. 1953. *The hydraulic geometry of stream channels and some physiographic implications*. Professional Paper 252, US Geological Survey, Reston, VA.

Leuven JRFW, Kleinhans MG, Weisscher SAH, van der Vegt M. 2016. Tidal sand bar dimensions and shapes in estuaries. *Earth-Science Reviews* **161**: 204–233.

Manning A. Enhanced UK estuaries database: explanatory notes and metadata, Technical Report TR167, HR Wallingford UK, 2007.

Meininger PL, Witte RH, Graveland J. Zeezoogdieren in de westerschelde: knelpunten en kansen, Technical Report 2003.041, Rijkswaterstaat, RIKZ Middelburg, 2003.

O'Brien MP. 1969. Equilibrium flow areas of inlets on sandy coasts. In *Journal of the waterways and harbors division: Proceedings of the American Society of Civil Engineers*, ASCE: Reston, VA; 43–52.

Pierik H, Cohen K, Stouthamer E. 2016. A new GIS approach for reconstructing and mapping dynamic late Holocene coastal plain palaeogeography. *Geomorphology* **270**: 55–70.

Pillsbury G. 1956. *Tidal Hydraulics*, rev. Corps of Engineers, US Army: Vicksburg, PA.

Repetto R, Tubino M. 2001. Topographic expressions of bars in channels with variable width. *Physics and Chemistry of the Earth, Part B: Hydrology, Oceans and Atmosphere* **26**(1): 71–76.

Sassi M, Hoitink A, Brye B, Deleersnijder E. 2012. Downstream hydraulic geometry of a tidally influenced river delta. *Journal of Geophysical Research: Earth Surface* **117**(F4): 1–13 F04022.

Savenije HH. 2003. The width of a bankfull channel; Lacey's formula explained. *Journal of Hydrology* **276**(1): 176–183.

Savenije HH. 2006. *Salinity and Tides in Alluvial Estuaries*. Elsevier: Amsterdam.

Savenije HH. 2015. Prediction in ungauged estuaries: an integrated theory. *Water Resources Research* **51**(4): 2464–2476.

Schramkowski G, Schuttelaars H, De Swart H. 2002. The effect of geometry and bottom friction on local bed forms in a tidal embayment. *Continental Shelf Research* **22**(11): 1821–1833.

Schuurman F, Marra WA, Kleinhans MG. 2013. Physics-based modeling of large braided sand-bed rivers: bar pattern formation, dynamics, and sensitivity. *Journal of Geophysical Research: Earth Surface* **118**(4): 2509–2527.

Seminara G. 2010. Fluvial sedimentary patterns. *Annual Review of Fluid Mechanics* **42**: 43–66.

Seminara G, Tubino M. 2001. Sand bars in tidal channels. Part 1. Free bars. *Journal of Fluid Mechanics* **440**: 49–74.

Shigemura T. 1980. Tidal prism–throat area relationships of the bays of Japan. *Shore and Beach* **48**(3): 30–35.

Struiksma N, Olesen K, Flokstra C, De Vriend H. 1985. Bed deformation in curved alluvial channels. *Journal of Hydraulic Research* **23**(1): 57–79.

Thomson A, Huiskes A, Cox R, Wadsworth R, Boorman L. 2004. Short-term vegetation succession and erosion identified by airborne remote sensing of Westerschelde salt marshes, The Netherlands. *International Journal of Remote Sensing* **25**(20): 4151–4176.

Toffolon M, Lanzoni S. 2010. Morphological equilibrium of short channels dissecting the tidal flats of coastal lagoons. *Journal of Geophysical Research: Earth Surface* **115**: 1–15 F04036.

Townend I. 2005. An examination of empirical stability relationships for UK estuaries. *Journal of Coastal Research* **21**: 1042–1053.

Townend I. 2012. The estimation of estuary dimensions using a simplified form model and the exogenous controls. *Earth Surface Processes and Landforms* **37**(15): 1573–1583.

Tubino M, Repetto R, Zolezzi G. 1999. Free bars in rivers. *Journal of Hydraulic Research* **37**(6): 759–775.

van den Berg JH, Jeuken CJ, Van der Spek AJ. 1996. Hydraulic processes affecting the morphology and evolution of the Westerschelde estuary. In *Estuarine Shores: Evolution, Environments and Human Alterations*, Nordstrom KF, Roman CT (eds), Wiley: Chichester; 157–184.

van der Spek AJ, Beets DJ. 1992. Mid-Holocene evolution of a tidal basin in the western Netherlands: a model for future changes in the northern Netherlands under conditions of accelerated sea-level rise? *Sedimentary Geology* **80**(3): 185–197.

van der Wal D, Wielemaker-Van den Dool A, Herman PM. 2008. Spatial patterns, rates and mechanisms of saltmarsh cycles (Westerschelde, The Netherlands). *Estuarine, Coastal and Shelf Science* **76**(2): 357–368.

van Eck GTM, Holzhauer H. Monitoring van de effecten van de verruiming 48'/43': Move eindrapport 2006 (rapport 10), Technical Report RIKZ/2007.003, Rijkswaterstaat Utrecht, 2007.

Vos P, de Koning J, Van Eerden R. 2015. Landscape history of the Oer-Ij tidal system, Noord-Holland (The Netherlands). *Netherlands Journal of Geosciences* **94**(04): 295–332.

Wood LJ. 2004. Predicting tidal sand reservoir architecture using data from modern and ancient depositional systems, integration of outcrop and modern analogs in reservoir modeling. *AAPG Memoir* **80**: 45–66.

Wu F-C, Shao Y-C, Chen Y-C. 2011. Quantifying the forcing effect of channel width variations on free bars: morphodynamic modeling based on characteristic dissipative Galerkin scheme. *Journal of Geophysical Research: Earth Surface* **116**(F3): 1–20.

Supporting Information

Additional supporting information may be found online in the supporting information tab for this article.

Copyright © 2017 John Wiley & Sons, Ltd.